

¹ Drought indices of water demand and supply, soil moisture, vegetation, and
² its impact on LULCC in continental Chile

³ Francisco Zambrano^{a,1,*}

^a Universidad Mayor, Hémera Centro de Observación de la Tierra, Facultad de Ciencias, Escuela de Ingeniería en Medio Ambiente y Sustentabilidad, Santiago, Chile, 7500994

⁴ **Abstract**

Human-induced greenhouse gas emissions have increased the frequency and/or intensity of weather and climate extremes. Central Chile has been affected by a persistent drought which is impacting the hydrological system and vegetation development. The region has been the focus of research studies due to the diminishing water supply, this persistent period of water scarcity has been defined as a “mega drought”. Nevertheless, our results evidence that the water deficit has expanded beyond. Our goal is to analyze the impact of drought, measured by drought indices of water supply/demand and vegetation status, in the LULCC (land use land cover change) over continental Chile. For the analysis, continental Chile was divided into five zones according to a latitudinal gradient: “Norte Grande”, “Norte Chico”, “Zona Central”, “Zona Sur”, and “Zona Austral”. We used monthly climatic re-analysis variables for precipitation, temperature and soil moisture for 1981-2023 from ERA5-Land (ERA5L); and MODIS (Moderate-Resolution Imaging Spectroradiometer) product MCD12Q1 for land cover for 2001-2021, and the NDVI vegetation index from product MOD13A2 collection 6.1 for 2000-2023, both from collection 6.1. We estimated atmospheric evaporative demand (AED) by combining the Hargreaves-Samani equation with the ERA5L temperature. We derived the drought indices SPI (Standardized Precipitation Index), SPEI (Standardized Precipitation Evapotranspiration Index), EDDI (Evaporative Demand Drought Index), SSI (standardized anomaly of cumulative soil moisture), and the zcNDVI (standardized anomaly of cumulative NDVI). These indices were calculated for time scales of 1, 3, 6, 12, 24, and 36 months, except for zcNDVI (1, 3, and 6 months). We analyzed the temporal correlation of SPI, SPEI, EDDI, and SSI with zcNDVI to have insights into the impact of water supply and demand on vegetation. Our results showed that LULCC had an increasing trend of 412 [km²yr⁻¹] of forest expansion in the “Zona Sur”, together with a decreasing trend of 24 [km²yr⁻¹] of cropland contraction in the “Zona Central” meanwhile the “Zona Sur” showed an increase of 31 [km²yr⁻¹], and a contraction of 80 [km²yr⁻¹] of bare soil in the “Zona Austral”. The EDDI was the less correlated index for the five macro zones and the five types of land cover, showing that the temperature in Chile has little impact on vegetation. Higher r-squared values, between 0.5 and 0.8, were obtained at “Norte Chico” and “Zona Central” for the land cover types of savanna, shrubland, grassland, and croplands for the indices SPEI and SSI at time scales of 12 and 24 months. The forest type reaches a r-squared of ~0.5 for SSI of 12 months. The results indicate that the “Norte Chico” and “Zona Central” are the most sensitive regions to water supply deficits longer than a year, potentially explained by a low capacity of water storage in those zones that should be further investigated.

⁵ **Keywords:** drought, land cover change, satellite

*Corresponding author

Email address: francisco.zambrano@umayor.cl (Francisco Zambrano)

¹This is the first author footnote.

6 **1. Introduction**

7 The sixth assessment report (AR6) of the IPCC (Calvin et al., 2023) indicates that human-induced green-
8 house gas emissions have increased the frequency and/or intensity of some weather and climate extremes,
9 and the evidence has been strengthened since AR5 (IPCC, 2013). There is high confidence that increasing
10 global warming can expand the land area affected by increasing drought frequency and severity (Seneviratne,
11 2021). Furthermore, drought increases tree mortality and triggers changes in land cover and, consequently,
12 land use, thus impacting ecosystems (Crausbay et al., 2017). Nevertheless, there is a lack of understanding
13 of how the alteration in water supply and demand is affecting land cover transformations.

14 Precipitation is the primary driver of drought and is intensified by temperature (Luo et al., 2017). Drought
15 impacts soil moisture, hydrological regimes, and vegetation productivity. Initially, drought was commonly
16 classified as meteorological, hydrological, and agricultural (Wilhite and Glantz, 1985). Lately, Van Loon
17 et al. (2016) and AghaKouchak et al. (2021) have given an updated definition of drought for the Anthro-
18 pocene, suggesting that it should be considered the feedback of humans' decisions and activities that drives
19 the anthropogenic drought. Even though it has been argued that those definitions do not fully address the
20 ecological dimensions of drought. Crausbay et al. (2017) proposed the ecological drought definition as "*an*
21 *episodic deficit in water availability that drives ecosystems beyond thresholds of vulnerability, impacts ecosystem*
22 *services, and triggers feedback in natural and/or human systems*". Moreover, many ecological studies
23 have misinterpreted how to characterize drought, for example, sometimes considering "dry" conditions as
24 "drought" (Slette et al., 2019). On the other hand, the AR6 (Calvin et al., 2023) states that even if global
25 warming is stabilized at 1.5°–2°C, many parts of the world will be impacted by more severe agricultural and
26 ecological droughts. Then, there is a challenge in conducting drought research, especially to evaluate its
27 impact on ecosystems.

28 Chile has been facing a persistent rainfall deficit for more than a decade (Garreaud et al., 2017), which
29 has impacted vegetation development (Zambrano, 2023) and the hydrological system (Boisier et al., 2018).
30 Current drought conditions have affected crop productivity (Zambrano et al., 2016, 2018), forest development
31 (Miranda et al., 2020; Venegas-González et al., 2018), forest fire occurrence (Urrutia-Jalabert et al., 2018),
32 land cover change (Fuentes et al., 2021), water supply in watersheds (Alvarez-Garreton et al., 2021), and
33 have had economic impacts (Fernández et al., 2023). In 2019–2020, the drought severity reached an extreme
34 condition in Central Chile (30–34°S) not seen for at least 40 years, and the evidence indicates that the
35 impact is transversal to the land cover classes of forest, grassland, and cropland (Zambrano, 2023). The
36 prolonged lack of precipitation in Central Chile is producing changes in ecosystem dynamics that must be
37 studied.

38 For the spatiotemporal assessment of drought impact (i.e., by water supply and demand) on land cover
39 changes, we need climatic reliable variables such as precipitation, temperature, soil moisture, land cover, and
40 vegetation status. For developing countries like Chile, the weather networks present several disadvantages,
41 such as gaps, a short history, and low-quality data. Reanalysis data, as the ERA5-Land (ERA5L) (Muñoz-
42 Sabater et al., 2021) provides hourly climatic information (precipitation, temperature, and soil moisture)
43 without gaps since 1950 with global extension. ERA5L has already been used for drought assessment using
44 the Standardized Precipitation-Evapotranspiration Index (SPEI) (Nouri, 2023) and for flash drought (Wang
45 et al., 2023) by analyzing soil moisture and evapotranspiration. On the other hand, satellite remote sensing
46 (West et al., 2019; AghaKouchak et al., 2015) is the primary method to evaluate how drought impacts
47 vegetation dynamics. Vegetation drought indices (VDI) are commonly used as proxies of productivity
48 (Paruelo et al., 2016; Schucknecht et al., 2017), which can be derived from the MODIS (Moderate-Resolution
49 Imaging Spectroradiometer). Besides, land use and land cover (LULC) change can be driven by drought
50 (Tran et al., 2019; Akinyemi, 2021). To analyze these changes, multiple LULC products exist (Grekousis
51 et al., 2015), one of those that provides time series since 2001 is the MCD12Q1 (Friedl and Sulla-Menashe,
52 2019) from MODIS. The variation in water supply and demand is finally reflected in the total water storage
53 (TWS). The TWS can be retrieved by the Gravity Recovery and Climate Experiment (GRACE), which
54 allows analyzing water availability changes at coarse resolution (Ahmed et al., 2014; Ma et al., 2017). We

55 can use climatic reanalysis (ERA5L) and vegetation data (MODIS) to derive drought indices of supply (i.e.,
56 precipitation) and demand (i.e., temperature) and thus evaluate the impact of drought on LULC changes.
57 Further, the TWS can be assessed with regard to the changes in water supply and demand to gain insight
58 into the impact on water storage.

59 To evaluate meteorological drought (i.e., water supply), the World Meteorological Organization (WMO;
60 [WMO et al. \(2012\)](#)) recommends the Standardized Precipitation Index (SPI; [McKee et al. \(1993\)](#)), a multi-
61 scalar drought index that allows to monitor precipitation deficits from short- to long-term. Following the
62 same approach, [Vicente-Serrano et al. \(2010\)](#) incorporates into the SPI the effect of temperature through
63 the use of potential evapotranspiration, thus proposing the SPEI (Standardized Precipitation Evapotranspi-
64 ration Index). Similarly, to evaluate solely the evaporative demand driven by temperature, [Hobbins et al.](#)
65 ([2016](#)) and [McEvoy et al. \(2016\)](#) came up with the Evaporative Demand Drought Index (EDDI). For veg-
66 etation, in a similar manner as the SPI, SPEI and EDDI; [Zambrano et al. \(2018\)](#) proposed the zcNDVI,
67 a standardized anomaly of the cumulative Normalized Difference Vegetation Index (NDVI), which could
68 be accumulated over the growing season or any period (e.g., months), resulting in a multiscalar drought
69 index. For soil moisture, several drought indices exist, such as the Soil Moisture Deficit Index (SDMI) a
70 normalized index ([Narasimhan and Srinivasan, 2005](#)) and the Soil Moisture Agricultural Drought Index
71 (SMADI) ([Souza et al., 2021](#)) which is a normalized index using vegetation, land surface temperature, and a
72 vegetation condition index (VCI, ([Kogan, 1995](#))). From TWS, we can estimate the standardized terrestrial
73 water storage index (STI) ([Cui et al., 2021](#)), a standardized anomaly that follows the methodology of the
74 SPI, SPEI, EDDI, and zcNDVI. Thereby, we have drought indices for water supply, demand, and storage,
75 which can help to make a comprehensive assessment of drought.

76 In this research, we present the raster dataset DDS4Chl, which provides climate variables and drought
77 indices of water demand and supply and vegetation productivity for continental Chile since 1981 at a
78 monthly frequency. Those were gathered from the earth observation products ERA5L and MODIS. Then,
79 we used DDS4Chl to analyze the impact of drought on different types of land cover classes in continental
80 Chile. The specific objectives of the study are: i) to analyze the trend on multi-scalar drought indices
81 for water demand and supply, soil moisture, and vegetation productivity for 1981–2023/2001–2023; ii) to
82 evaluate LULC change for 2001–2021 and its relation to drought indices; iii) to analyze the relationship of
83 a proxy of vegetation productivity (zcNDVI) with drought indices of water demand and supply and soil
84 moisture; and iv) to assess if the observed changes in the drought indices are linked to TWS.

85 **2. Study area (AGREGAR SUPERFICIE DE LANDCOVER EN CADA MACROZONA)**

86 Continetal Chile has a diverse climate condition from north to south and east to west ([Aceituno et al.,](#)
87 [2021](#)) (Figure 1), which determines its great ecosystem diversity (Figure 2). The Andes Mountains are a
88 main factor in latitudinal variation ([Garreaud, 2009](#)). To describe the climate and ecosystem of Chile, we
89 use the Koppen-Geiger release by [Beck et al. \(2023\)](#) and the landcover type persistance of 80% of times
90 for 2001–2022, from the IGBP classification scheme ([Friedl and Sulla-Menashe, 2019](#)) (see Section 3.4).
91 “Norte Grande” and “Norte Chico” predominate in an arid desert climate with hot (Bwh) and cold (Bwk)
92 temperatures. At the south of “Norte Chico,” the climate changes to an arid steppe with cold temperatures
93 (Bsk). Mainly, the land is barren, with a minor surface of vegetation types such as shrubland and grassland.
94 In the zones “Centro” and the north half of “Sur,” the main climate is Mediterranean, with warmer to hot
95 summers (Csa and Csb). In “Centro,” there is a major proportion (~50%) of Chilean matorral (shrubland
96 and savanna, ([Fuentes et al., 2021](#))), followed by grassland (~16%), forest (8%), and croplands (5%). The
97 south part of “Sur” and the north part of “Austral” are dominated by an Oceanic climate (Cfb). Those zones
98 are high in forest and grassland. The southern part of the country has a tundra climate, and in Patagonia,
99 it is a cold semi-arid area with an extended surface of grassland, forest, and, to a lesser extent, savanna.

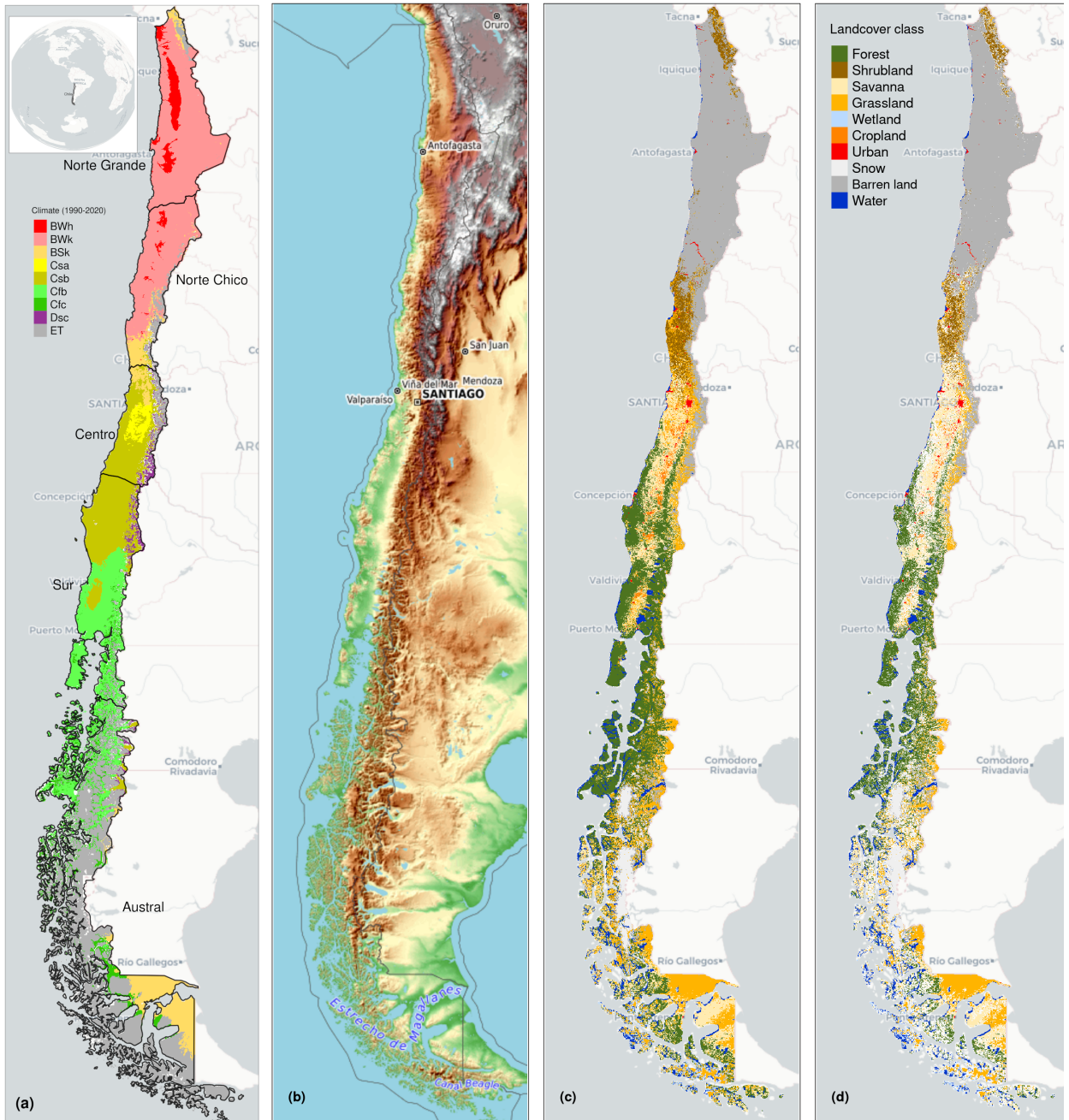


Figure 1: (a) Chile with the Koppen-Geiger climate classes and the five macrozones “Norte Grande”, “Norte Chico”, “Centro”, “Sur”, and “Austral”. (b) Topography reference map. (c) Land cover classes for 2022. (d) Persistent land cover classes (> 80%) for 2001-2022

100 3. Materials and Methods

101 3.1. Software and packages used

102 For the downloading, processing, and analysis of the spatio-temporal data, we used the open source software
 103 for statistical computing and graphics, R ([R Core Team, 2023](#)). For downloading ERA5L, we used the
 104 `{ecmwfr}` package ([Hufkens et al., 2019](#)). For processing raster data, we used `{terra}` ([Hijmans, 2023](#)) and

¹⁰⁵ `{stars}` (Pebesma and Bivand, 2023). For managing vectorial data, we used `{sf}` (Pebesma, 2018). For
¹⁰⁶ the calculation of AED, we used `{SPEI}` (Beguería and Vicente-Serrano, 2023).

¹⁰⁷ *3.2. Data*

¹⁰⁸ *3.2.1. Earth observation data*

¹⁰⁹ For water supply and demand variables, we used ERA5L (Muñoz-Sabater et al., 2021), a reanalys dataset
¹¹⁰ that provides the evolution of land variables since 1950. It has a spatial resolution of 0.1°, hourly frequency,
¹¹¹ and global coverage. We selected the variables for total precipitation, 2 meter temperature maximum and
¹¹² minimum, and volumetric soil water layers between 0 and 100cm of depth (layer 1 to layer 3). The data
¹¹³ was downloaded using the Copernicus Climate Data Store (CDS) Application Program Interface (API)
¹¹⁴ implemented in `{ecmwf}` (Hufkens et al., 2019).

¹¹⁵ To derive a proxy of vegetation productivity, we used the product MOD13A3 collection 6.1 from MODIS
¹¹⁶ (Didan, 2015). It provides vegetation indices (NDVI and EVI) at 1km of spatial resolution and monthly
¹¹⁷ frequency. The MOD13A3.061 and MCD12Q1.061 were retrieved from the online Data Pool, courtesy of
¹¹⁸ the NASA EOSDIS Land Processes Distributed Active Archive Center (LP DAAC), USGS Earth Resources
¹¹⁹ Observation and Science (EROS) Center, Sioux Falls, South Dakota, <https://lpdaac.usgs.gov/tools/data-pool/>.

Table 1: Description of the earth observation data used

Product	Sub-product	Variable	Spatial Resolution	Period	Units	Short Name
ERA5L		Precipitation	0.1°	1981-2023	mm	P
		Maximum temperature			°C	T_{max}
		Minimum temperature			°C	T_{min}
		Volumetric Soil Water Content at 1m			m3/m3	SM
ERA5L*	MOD13A3.061	Atmospheric Evaporative Demand	0.1°	1981-2023	mm	AED
MODIS		Normalized Difference Vegetation Index	1 km	2000-2023		NDVI
		Landcover IGBP scheme		2001-2022		Landcover

*Derived from ERA5L with Eq. 1.

¹²¹ *3.2.2. in-situ data*

¹²² *3.2.3. Validation of ERA5L variables*

¹²³ *3.3. Drought Indices*

¹²⁴ We derived the drought indices of water supply and demand, soil moisture from the ERA5L dataset, and
¹²⁵ vegetation from the MODIS product, all at monthly frequency.

¹²⁶ *3.3.1. Atmospheric Evaporative Demand (AED)*

¹²⁷ For the indices EDDI and SPEI that use water demand, first we have to calculate the AED. For this, we
¹²⁸ used the method of Hargreaves (Hargreaves, 1994):

$$AED = 0.0023 \cdot Ra \cdot (T + 17.8) \cdot (T_{max} - T_{min})^{0.5} \quad (1)$$

¹²⁹ where Ra ($MJ\ m^2\ day^{-1}$) is extraterrestrial radiation; T , T_{max} , and T_{min} are mean, maximum, and
¹³⁰ minimum temperature ($^{\circ}C$). We calculate the centroid coordinates per pixel and use the latitude to estimate
¹³¹ Ra .

132 3.3.2. Non-parametric calculation of drought indices

133 To evaluate water demand, we chose the *EDDI* (Hobbins et al., 2016; McEvoy et al., 2016) index, which
 134 uses the *AED*. For supply, we used the index recommended by the World Meteorological Organization
 135 (WMO) for monitoring drought, the *SPI* (McKee et al., 1993). We calculated the *SPEI*, which used a
 136 balance between *P* and *AED*, in this case, an auxiliary variable $D = P - AED$ is used. In this study,
 137 we used the *SSI* (standardized soil moisture index at 1 m) (Hao and AghaKouchak, 2013; AghaKouchak,
 138 2014), which uses *SM*. Finally, for the proxy of productivity, *zcNDVI*, we used the *NDVI*. Before using the
 139 *NDVI*, it was smoothed using a locally-weighted polynomial regression, following the procedure described
 140 in Zambrano et al. (2018) and Zambrano et al. (2016).

141 All the indices are multi-scalar and were calculated for time scales of 1, 3, 6, 12, 24, and 36 months, except
 142 for *zcNDVI*, which was calculated for 6 months. The goal is to be able to evaluate short- and long-term
 143 droughts in water demand and supply and soil moisture. This is particularly important for central Chile
 144 because it has suffered from a prolonged decrease in precipitation for more than 12 years (Garreaud et al.,
 145 2020; Boisier et al., 2018; Garreaud et al., 2017).

146 To calculate the drought indices, first we must calculate the accumulation of the variable. In this case, for
 147 generalization purposes, we will use *V*, referring to *P*, *AED*, *D*, *NDVI*, and *SM* (Table 1). We cumulated
 148 each *V* over the time series of *n* values, and for the time scales *s*:

$$A_{si} = \sum_{i=n-s-i+2}^{n-i+1} V_i \quad \forall i \geq n-s+1 \quad (2)$$

149 It corresponds to a moving window (convolution) that sums the variable for *s* starting for the last month
 150 *n* until the month, which could sum for *s* months (*n*-*s*+1). Once the variable is cumulated over time
 151 for the scale *s*, we used a nonparametric approach following Hobbins et al. (2016) to derive the drought
 152 indices. Thus, the empirically derived probabilities are obtained through an inverse normal approximation
 153 (Abramowitz and Stegun, 1968). Then, we used the empirical Tukey plotting position (Wilks, 2011) over
 154 A_i to derive the $P(A_i)$ probabilities across a period of interest:

$$P(A_i) = \frac{i - 0.33}{n + 0.33} \quad (3)$$

155 The drought indices *SPI*, *SPEI*, *EDDI*, *SSI*, and *zcNDVI* are obtained following the inverse normal
 156 approximation:

$$DI(A_i) = W - \frac{C_0 + C_1 \cdot W + c_2 \cdot W^2}{1 + d_1 \cdot W + d_2 \cdot W^2 + d_3 \cdot W^3} \quad (4)$$

157 *DI* is referring to the drought index calculated for the variable *V*. The values for the constants are:
 158 $C_0 = 2.515517$, $C_1 = 0.802853$, $C_2 = 0.010328$, $d_1 = 1.432788$, $d_2 = 0.189269$, and $d_3 = 0.001308$. For
 159 $P(A) \leq 0.5$, $W = \sqrt{-2 \cdot \ln(P(A))}$, and for $P(A_i) > 0.5$, replace $P(A_i)$ with $1 - P(A_i)$ and reverse the sign
 160 of $DI(A_i)$.

161 3.4. LULC change for 2001-2022 and its relation with water supply and demand, and soil moisture

162 To analyze the LULCC, we use the IGBP scheme from the MCD12Q1 collection 6.1 from MODIS. This
 163 product has a yearly frequency from 2001 to 2022. The IGBP defines 17 classes; from these, we regrouped
 164 into ten macroclasses for forest, shrublands, savannas, grasslands, wetlands, croplands, urban, snow and
 165 ice, barren, and water bodies. To validate the IGBP MODIS, we compare the macroclasses with the ones of
 166 a more detailed landcover map made by Zhao et al. (2016) for Chile for the years 2013–2014 (LCChile). The
 167 later has a spatial resolution of 30 m and three levels of defined classes; from those, we used level 1, which

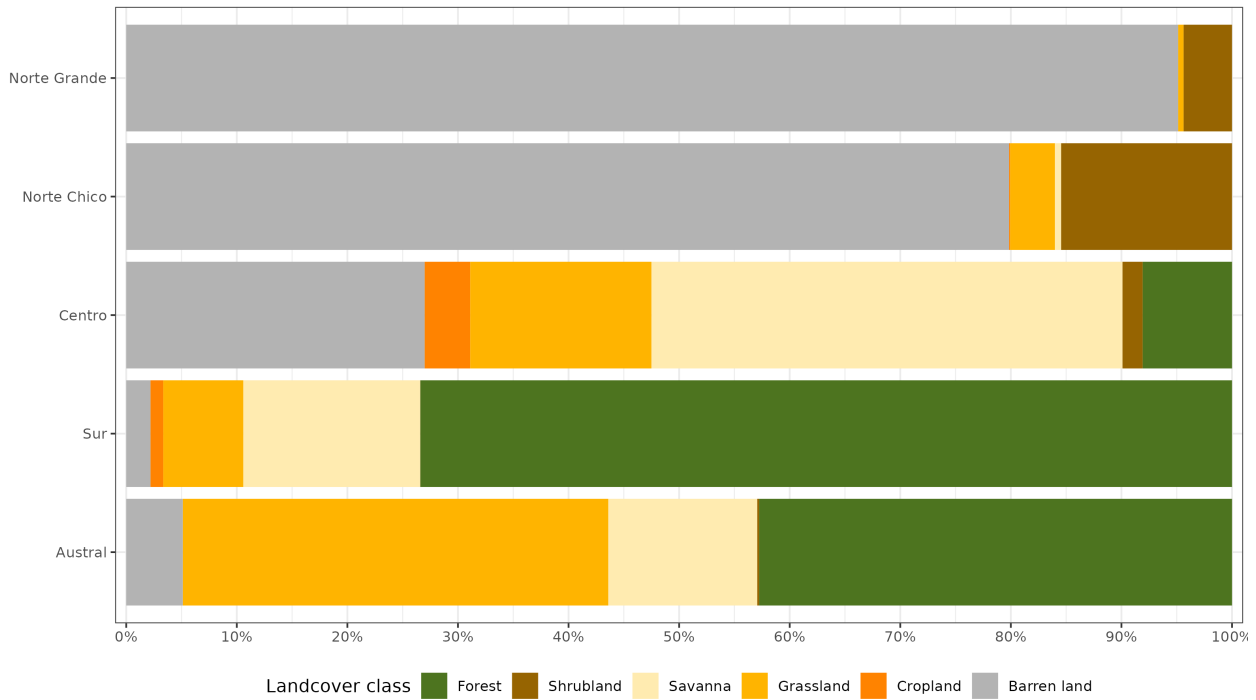


Figure 2: Proportion of land cover class from the persistent land cover for 2001-2022 (>80%) per macrozone

fits with the macroclasses derived from the IGBP MODIS. We chose the years 2013 and 2014 from MODIS IGBP because the LCChile was made with data acquired in 2013 and 2014. We resampled LCChile to the spatial resolution of the IGBP MODIS using the nearest neighbor method. Then, we took a random sample of 1000 points within continental Chile and extracted the classes that fell within each point for LCCHILE, IGP2013, and IGBP2014. Finally, we applied a confusion matrix and estimated the accuracy and F1 score as metrics of performance. The validation of IGBP2013 and IGBP2014 with LCChile reached similar metrics of performance, having an accuracy of 0.82 and a F1 score of 0.66 (see SS1).

Later, with the goal of analyzing vegetation areas less affected by landcover change, we calculated a raster mask for IGBP MODIS considering the classes that remain for more than 80% of the years (2001–2022), which allows us to identify the areas with no landcover change for the macroclasses. Figure 2 shows the summary of the proportion of surface per landcover class and macrozone, derived from the mask over continental Chile.

Further, we calculated the surface occupied per landcover class into the five macrozones (“Norte Grande” to “Austral”) per year. After that, we calculated the trend’s change in surface; we used the Sen’ slope (Sen, 1968) based on Mann-Kendall (Kendall, 1975). This way, we obtain a matrix of trends of 5 x 5 (macrozones x landcover).

We will explore if the trend in landcover classess is associated to trend of the drought indices. For this we will use the regularizations techniques of Lasso (Tibshirani et al., 2010) and Ridge regression (Hoerl and Kennard, 1970). Also, we will test random forest for this purpose (Ho, 1995).

3.5. Trend of drought indices for water demand and supply, soil moisture, and vegetation productivity

To estimate if there are significant positive or negative trends for the drought indices, we used the non-parametric test of Mann-Kendall (Kendall, 1975). To determine the magnitude of the trend, we used Sen’s slope (Sen, 1968). One of the advantages of applying this methodology is that the Sen’s slope is not affected

191 by outliers as regular regression does. We applied both to the six time scales from 1981 to 2023 (monthly
192 frequency) and the indices SPI, EDDI, SPEI, and SSI. In the case of zcNDVI (six months) was for 2000 to
193 2023. Thus, we have 31 trends. Also, we extracted the trend aggregated by macrozone and landcover class,
194 obtaining a table of 31x5x5 (drought indices trends x macrozone x landcover class). We will use this data in
195 Section 3.4 to analyze if there is a strong relationship between the trends of drought indices and land cover
196 surface within continental Chile.

197 For zcNDVI, we want to remove the effect of the Andes's mountain and mask out trends that were at an
198 elevation above 1500m because there is scarce vegetation.

199 [Vicente-Serrano et al. \(2022\)](#) made a global analysis of the drought's severity trend using SPI, SPEI, and
200 the Standardized Evapotranspiration Deficit Index (SEDI; [Vicente-Serrano et al. \(2018\)](#)) to evaluate AED.
201 They indicate that the increase in hydrological drought has been due to anthropogenic effects rather than
202 climate change. This is because the global increase in AED did not explain the change in the spatial pattern
203 of the hydrological drought. Also, they state that "*the increase in hydrological droughts has been primarily
204 observed in regions with high water demand and land cover change*". We will contrast this hypothesis with
205 what is occurring in Chile. To achieve this, we will use the landcover class type that remains more than
206 80% of types for 2001–2022 to evaluate the trend on zcNDVI and use this as a mask where there are low
207 changes.

208 3.6. Impact for water supply and demand, and soil moisture in vegetation productivity within landcover types

209 The aim of this section is to analyze the drought indices of water demand and supply and soil moisture
210 against vegetation to address: i) if short- or long-term time scales are most important in impacting vegetation
211 through Chile; and ii) the strength of the correlation for the variable and the time scale. Then, we will
212 summarize for each landcover class and macrozone. Thus, we will be able to advance in understanding how
213 climate is affecting vegetation, considering the impact on the five macroclasses: forest, cropland, grassland,
214 savanna, and shrubland.

215 To assess how water demand and supply and soil moisture are related to vegetation productivity (zcNDVI),
216 we analyze the linear correlation between the indices SPI, SPEI, EDDI, and SSI for 1, 3, 6, 12, 24, and
217 36-month time scales against zcNDVI. We followed a similar approach to that used by [Meroni et al. \(2017\)](#)
218 when using the SPI for meteorological drought against the cumulative FAPAR (Fraction of Absorbed Pho-
219 tosynthetically Active Radiation) as a proxy for vegetation productivity. We made a pixel-to-pixel linear
220 correlation analysis per index. First, we calculate the Pearson coefficient of correlation for the six time scales
221 and let the time scale that reaches the maximum correlation be significant ($p < 0.05$). Then, we extracted
222 the Pearson correlation value corresponding to the time scales that reached the maximum value. Thus, we
223 derived two raster maps per index, the first with the time scales and the second with the correlation value.

224 4. Results

225 4.1. LULC change for 2001-2022 and its relation with water supply and demand, and soil moisture

226 Figure 3 and Table 2 show that the macrozones with major LULCC for 2001-2022 were "Centro", "Sur",
227 and "Austral" with 36%, 31%, and 34%, respectively. The "Norte Chico" shows an increase in barren land
228 of $111 \text{ km}^2 \text{year}^{-1}$ and a reduction in the class savanna $-70 \text{ km}^2 \text{year}^{-1}$. In the "Centro" and "Sur" there
229 are changes in the Chilean matorral, with an important reduction in savanna (-136 to $-318 \text{ km}^2 \text{yr}^{-1}$), and
230 an increase in shrubland and grassland. Showing a change for more dense vegetation types. It appears to
231 be a change from the surface occupied by cropland from the "Centro" to the "Sur." Also, there is a high
232 increase in forest ($397 \text{ km}^2 \text{yr}^{-1}$) in the "Sur," replacing the savanna lost.

233 4.2. Trend of drought indices for water demand and supply, soil moisture, and vegetation productivity

234 Regarding vegetation productivity aggregated through the macrozones in the five landcover macroclasses.
235 In "Norte Grande" there is a increase trend of 0.02 (z-index) per decade, related with types of grassland

Table 2: The value of Sen’s slope trend next to the time-series plot of surface per landcover class (IGBP MCD12Q1.016) for 2001–2022 through Central Chile. Values of zero indicate that there was not a significant trend. Red dots on the plots indicate the maximum and minimum values of surface.

macrozone	Trend of change [$\text{km}^2 \text{ year}^{-1}$]											
	Forest		Cropland		Grassland		Savanna		Shrubland		Barren land	
	x	y	x	y	x	y	x	y	x	y	x	y
Norte Grande								0.0			0.0	0.0
Norte Chico					-12.1			0.0		-70.0		111.2
Centro		0.0			-22.4		83.2		-136.2		146.0	22.9
Sur		396.6			37.8		0.0		-318.8			0.0
Austral		0.0					0.0		172.1		-36.9	-93.2

236 and shrubland. There is a negative trend in “Norte Chico” with -0.04 and “Centro” with -0.02 per decade.
237 In the “Norte Chico,” savanna (-0.05) has the lowest trend, and the rest of the types are around -0.04. In
238 “Centro,” shrubland reaches -0.06, followed by grassland with -0.05, and croplands and savanna have ~ 0.01
239 per decade. This could be associated either with a reduction in vegetation surface, a decrease in biomass,
240 or browning (Miranda et al., 2023). Vegetation reached its lowest values since the year 2019, reaching an
241 extreme condition in early 2020 and 2022 in the “Norte Chico” and Centro” (Mega Drought). The “Sur”
242 and “Austral” show a positive trend of around 0.016 per decade (Figure 3). The area most affected by a
243 negative trend in vegetation seems to be associated with the Chilean matorral (Fuentes et al., 2021), despite
244 the croplands being as severely impacted by drought as native vegetation does in “Norte Chico.”

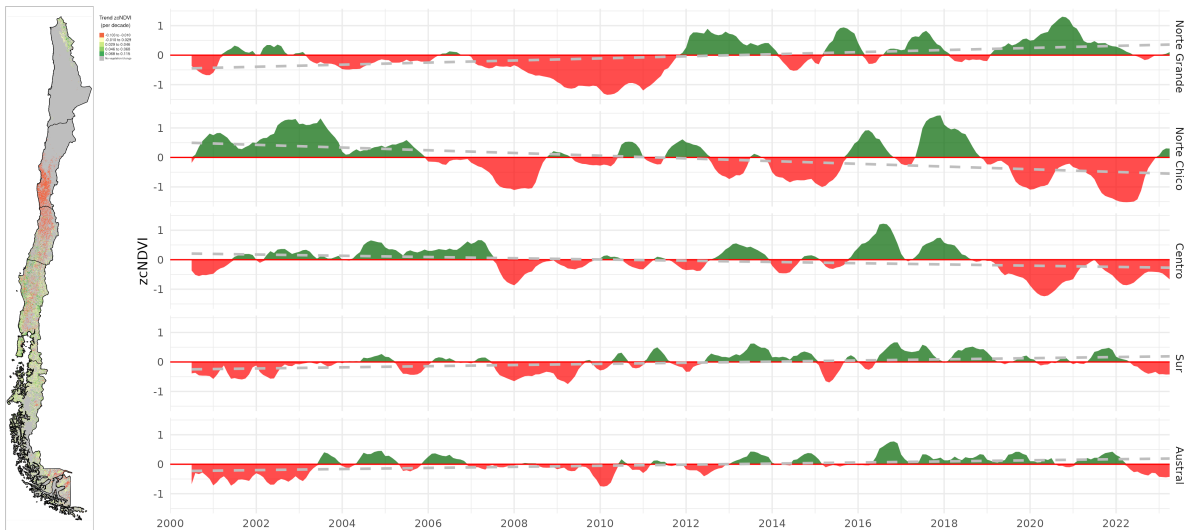


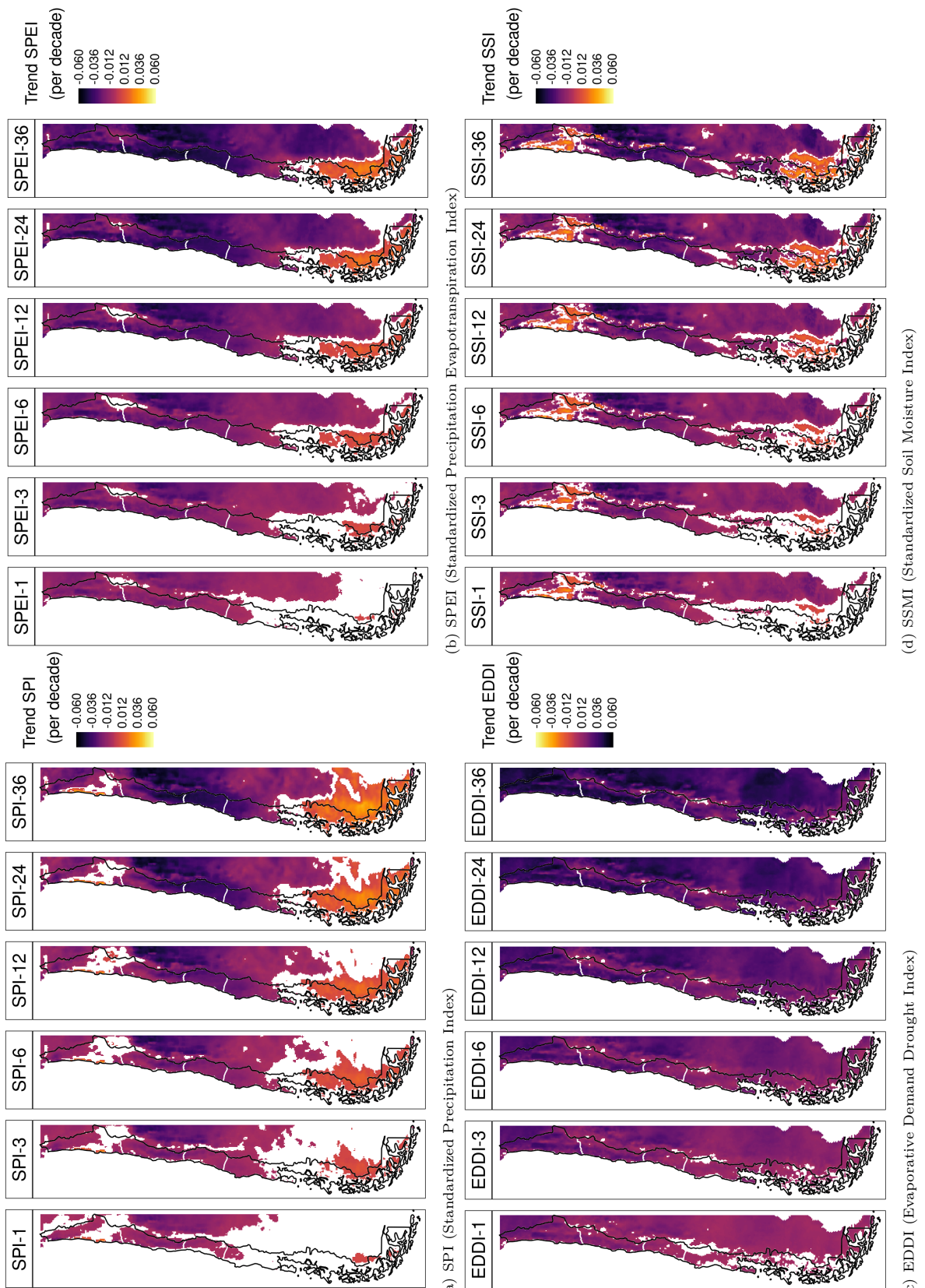
Figure 3: (a) Map of the linear trend of the index zcNDVI-6 for 2001–2023. Greener colors indicate a positive trend; red colors correspond to a negative trend and a decrease in vegetation productivity. Grey colors indicate either no vegetation or a change in landcover type for 2001–2022. (b) Temporal variation of zcNDVI-6 aggregated at macrozone level within continental Chile. Each horizontal panel corresponds to a macrozone from ‘Norte Grande’ to ‘Austral’.

245 Analyzing the water supply, the macrozones that have the lowest trend are “Norte Chico” and “Centro,”
246 where the SPI, SPEI, and SSI show that it decreases at longer time scales due to the prolonged reduction in
247 precipitation. At 36 months, it reaches trends between -0.03 and -0.04 (z-score) per decade for SPI, SPEI,
248 and SSI (Figure 4). For “Sur,” the behavior is similar, decreasing at longer scales and having between -0.016
249 and -0.025 per decade for SPI, SPEI, and SSI. On the other hand, all macrozones show an increase in the

250 trend in all the drought indices, with “Norte Grande” having the highest at 36 months (0.042 per decade).
251 Because of this, the SPEI (which uses AED) reached its lowest value in “Norte Grande,” with -0.03 at 36
252 months. Despite the other macrozones, “Austral” showed an increase in all indices, being the highest for
253 EDDI at 36 months (0.025) and the lowest for SSI, which shows only a minor increase in the trend (Figure 4).

254 *4.3. Impact for water supply and demand, and soil moisture in vegetation productivity*

255 According to what is shown in Figure 5, Figure 6, and Table 3, forest seems to be the most resistant type
256 to drought. Showing that only “Centro” is slightly ($rsq = 0.25$) impacted by a 12-month soil moisture deficit
257 (SSI-12). Grasslands are shown to be impacted by a SSI-12 with a $rsq = 0.45$ and by a decrease in water
258 supply (SPI-36 and SPEI-24 with $rsq = 0.28$ and 0.34, respectively) in the “Norte Chico” and to a lesser
259 degree in the “Norte Grande.” But, in further south macrozones, this type was not affected by water demand,
260 water supply, or soil moisture. The types that show to be most affected by variation in climate conditions
261 are shrublands, savannas, and croplands. For savannas in “Norte Chico,” the SSI-12 and SPI-24 reached
262 an rsq of 0.74 and 0.58, respectively. This value decreases to the south, but the SSI-12 is still the variable
263 explaining more of the variation in vegetation productivity ($rsq = 0.45$ in “Centro” and 0.2 in “Sur”). In the
264 case of croplands, the SPEI-12, SPI-36, and SSI-12 explain between 45% and 66% of “Norte Chico.” The
265 most affected type by climatic variation was shrubland, where in “Norte Chico” and “Centro” soil moisture
266 explained 59% and precipitation, 37%, with SSI-12 being the most relevant variable, followed by SPI-36 in
267 “Norte Chico” and SPI-24 in “Sur.”

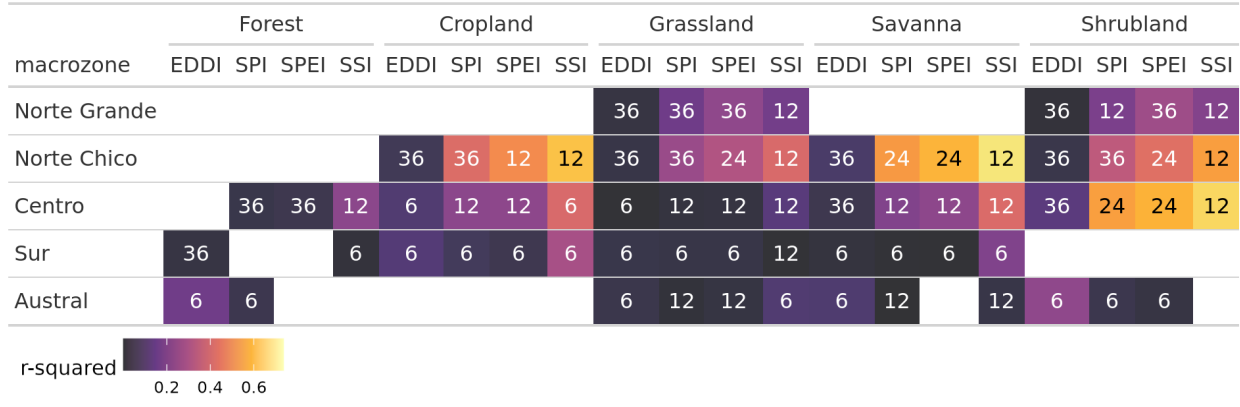


(c) EDDI (Evaporative Demand Drought Index)

(d) SSMI (Standardized Soil Moisture Index)

Figure 4: Linear trend of the drought index (*) at time scales of 1, 3, 6, 12, 24, and 36 months for 1981-2023

Table 3: Summary per landcover macroclass and macrozone regarding the correlation between zcNDVI with the drought indices EDDI, SPI, SPEI, and SSI for time scales of 1, 3, 6, 12, 24, and 36. The numbers in each cell indicate the time scale that reached the maximum correlation for the landcover and macrozone, and the color indicates the strength of the r-squared obtained with the index and the time scale.



268 *4.4. Validation of ERA5L variables*

269 *5. Discussion*

270 1.- Respecto a lo que indica [Vicente-Serrano et al. \(2018\)](#), de que el aumento en la tendencia en severidad
271 de la sequía (hidrológica) tiene que ver más con un aumento de la demanda de agua (LULCC) que a una
272 tendencia en las condiciones climáticas (SPI-12).

273 2.- Sobre los tipos de landcover más afectados por los indicadores de sequía. Asociación con el matorral
274 chileno ([Fuentes et al., 2021](#)). Diferencia entre el Norte Chico y Centro y lo que pasa hacia el sur.

275 3. Como podrían servir estos resultados para desarrollar un predictor de sequía basado.

276 4.- Qué se podría hacer mejor en futuras investigaciones del tema.

277 5.- Sequía, aridez, water scarcity (?) Si puede utilizar el mapa y proyección climática de Koppen_Geiger
278 ([Beck et al., 2023](#)) para dirigir esta discusión

279 *6. Conclusion*

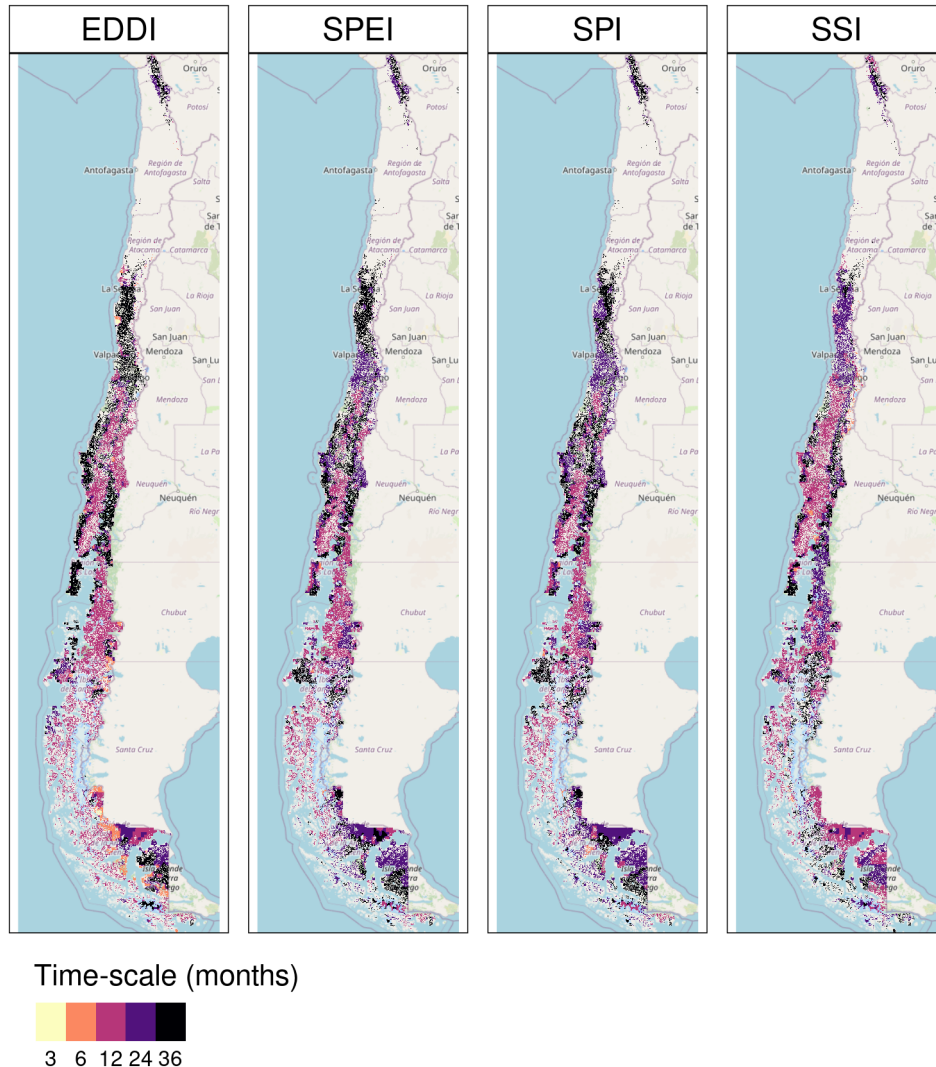


Figure 5: Time scales per drought index that reach the maximum coefficient of determination

280 References

- 281 Abramowitz, M., Stegun, I.A., 1968. Handbook of mathematical functions with formulas, graphs, and mathematical tables. 282 volume 55. US Government printing office.
- 283 Aceituno, P., Boisier, J.P., Garreaud, R., Rondanelli, R., Ruttlant, J.A., 2021. Climate and Weather in Chile, in: Fernández, 284 B., Gironás, J. (Eds.), Water Resources of Chile. Springer International Publishing, Cham. volume 8, pp. 7–29. URL: 285 http://link.springer.com/10.1007/978-3-030-56901-3_2.
- 286 AghaKouchak, A., 2014. A baseline probabilistic drought forecasting framework using standardized soil moisture index: application to the 2012 United States drought. Hydrology and Earth System Sciences 18, 2485–2492. URL: 287 <https://hess.copernicus.org/articles/18/2485/2014/>, doi:[10.5194/hess-18-2485-2014](https://doi.org/10.5194/hess-18-2485-2014).
- 288 AghaKouchak, A., Farahmand, A., Melton, F.S., Teixeira, J., Anderson, M.C., Wardlow, B.D., Hain, C.R., 2015. Remote 289 sensing of drought: Progress, challenges and opportunities. Reviews of Geophysics 53, 452–480. URL: <http://dx.doi.org/10.1002/2014RG000456>, doi:[10.1002/2014RG000456](https://doi.org/10.1002/2014RG000456).
- 290 AghaKouchak, A., Mirchi, A., Madani, K., Di Baldassarre, G., Nazemi, A., Alborzi, A., Anjileli, H., Azarderakhsh, M., Chiang, 291 F., Hassanzadeh, E., Huning, L.S., Mallakpour, I., Martinez, A., Mazdiyasni, O., Moftakhar, H., Norouzi, H., Sadegh, 292 M., Sadeqi, D., Van Loon, A.F., Wanders, N., 2021. Anthropogenic Drought: Definition, Challenges, and Opportunities. 293 Reviews of Geophysics 59, e2019RG000683. URL: <https://agupubs.onlinelibrary.wiley.com/doi/10.1029/2019RG000683>, doi:[10.1029/2019RG000683](https://doi.org/10.1029/2019RG000683).
- 294 Ahmed, M., Sultan, M., Wahr, J., Yan, E., 2014. The use of GRACE data to monitor natural and anthropogenic induced 295

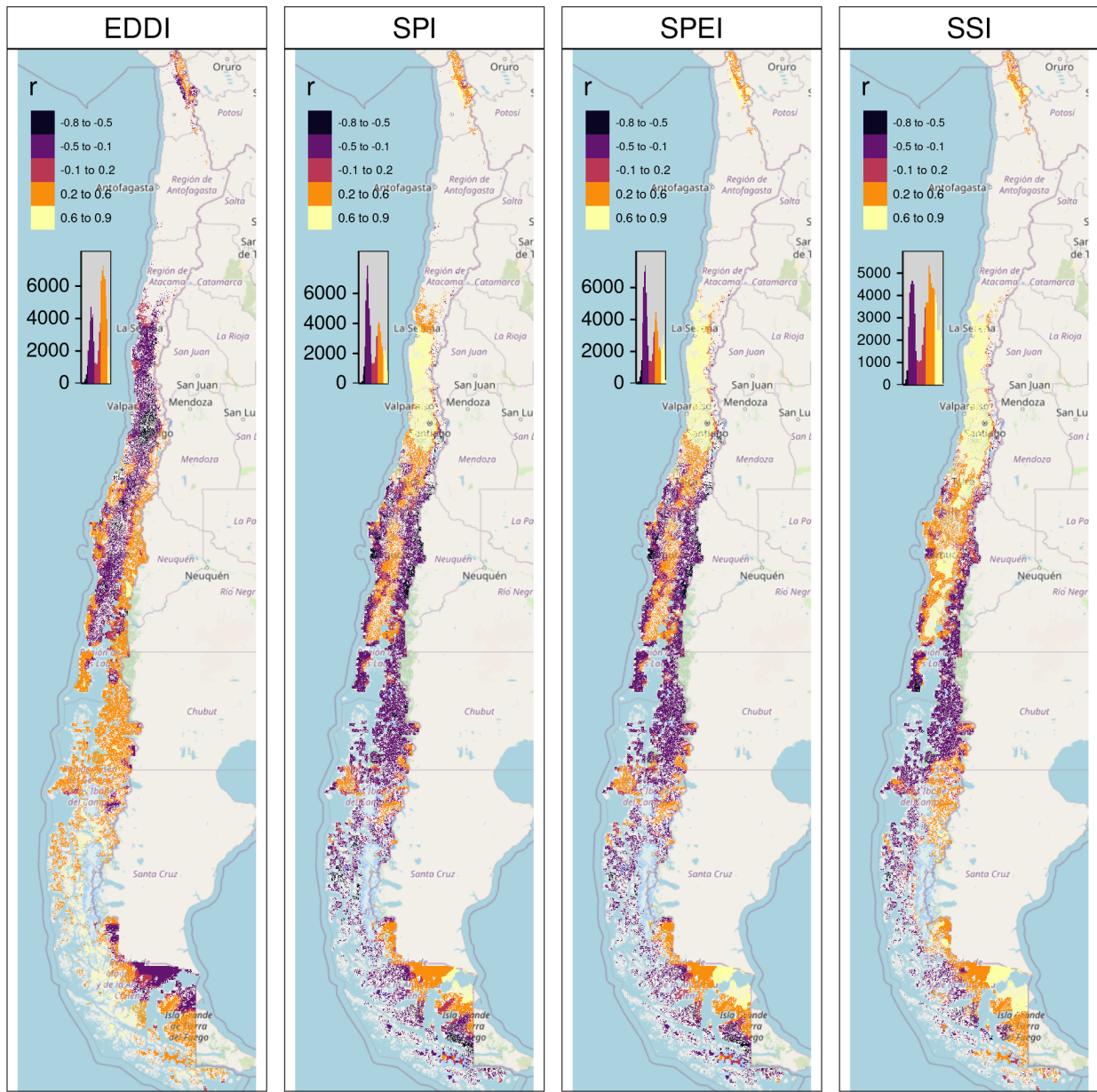


Figure 6: Pearson correlation value for the time scales and drought index that reach the maximum coefficient of determination

- 298 variations in water availability across Africa. *Earth-Science Reviews* 136, 289–300. doi:[10.1016/J.EARSCIREV.2014.05.009](https://doi.org/10.1016/J.EARSCIREV.2014.05.009).
299 publisher: Elsevier.
- 300 Akinyemi, F.O., 2021. Vegetation Trends, Drought Severity and Land Use-Land Cover Change during the Growing Season in
301 Semi-Arid Contexts. *Remote Sensing* 2021, Vol. 13, Page 836 13, 836. URL: <https://www.mdpi.com/2072-4292/13/5/836/> htm, doi:[10.3390/RS13050836](https://doi.org/10.3390/RS13050836). publisher: Multidisciplinary Digital Publishing Institute.
- 303 Alvarez-Garreton, C., Boisier, J.P., Garreaud, R., Seibert, J., Vis, M., 2021. Progressive water deficits during multiyear
304 droughts in basins with long hydrological memory in Chile. *Hydrology and Earth System Sciences* 25, 429–446. URL:
305 <https://hess.copernicus.org/articles/25/429/2021/>, doi:[10.5194/hess-25-429-2021](https://doi.org/10.5194/hess-25-429-2021).
- 306 Beck, H.E., McVicar, T.R., Vergopolan, N., Berg, A., Lutsko, N.J., Dufour, A., Zeng, Z., Jiang, X., van Dijk, A.I.J.M., Miralles,
307 D.G., 2023. High-resolution (1 km) Köppen-Geiger maps for 1901–2099 based on constrained CMIP6 projections. *Scientific
308 Data* 10. URL: <http://dx.doi.org/10.1038/s41597-023-02549-6>, doi:[10.1038/s41597-023-02549-6](https://doi.org/10.1038/s41597-023-02549-6).
- 309 Beguería, S., Vicente-Serrano, S.M., 2023. SPEI: Calculation of the Standardized Precipitation-Evapotranspiration Index. URL:

310 <https://CRAN.R-project.org/package=SPEI>.
 311 Boisier, J.P., Alvarez-Garreton, C., Cordero, R.R., Damiani, A., Gallardo, L., Garreaud, R.D., Lambert, F., Ramallo, C.,
 312 Rojas, M., Rondanelli, R., 2018. Anthropogenic drying in central-southern Chile evidenced by long-term observations
 313 and climate model simulations. *Elementa* 6, 74. URL: <https://www.elementascience.org/article/10.1525/elementa.328/>,
 314 doi:[10.1525/elementa.328](https://doi.org/10.1525/elementa.328).
 315 Calvin, K., Dasgupta, D., Krinner, G., Mukherji, A., Thorne, P.W., Trisos, C., Romero, J., Aldunce, P., Barrett, K., Blanco,
 316 G., Cheung, W.W., Connors, S., Denton, F., Diongue-Niang, A., Dodman, D., Garschagen, M., Geden, O., Hayward, B.,
 317 Jones, C., Jotzo, F., Krug, T., Lasco, R., Lee, Y.Y., Masson-Delmotte, V., Meinshausen, M., Mintenbeck, K., Mokssit, A.,
 318 Otto, F.E., Pathak, M., Pirani, A., Poloczanska, E., Pörtner, H.O., Revi, A., Roberts, D.C., Roy, J., Ruane, A.C., Skea,
 319 J., Shukla, P.R., Slade, R., Slangen, A., Sokona, Y., Sörensson, A.A., Tignor, M., Van Vuuren, D., Wei, Y.M., Winkler,
 320 H., Zhai, P., Zommers, Z., Hourcade, J.C., Johnson, F.X., Pachauri, S., Simpson, N.P., Singh, C., Thomas, A., Totin, E.,
 321 Arias, P., Bustamante, M., Elgizouli, I., Flato, G., Howden, M., Méndez-Vallejo, C., Pereira, J.J., Pichs-Madruga, R., Rose,
 322 S.K., Saheb, Y., Sánchez Rodríguez, R., Ürge Vorsatz, D., Xiao, C., Yassa, N., Alegría, A., Armour, K., Bednar-Friedl, B.,
 323 Blok, K., Cissé, G., Dentener, F., Eriksen, S., Fischer, E., Garner, G., Guivarc, C., Haasnoot, M., Hansen, G., Hauser, M.,
 324 Hawkins, E., Hermans, T., Kopp, R., Leprince-Ringuet, N., Lewis, J., Ley, D., Ludden, C., Niamir, L., Nicholls, Z., Some,
 325 S., Szopa, S., Trewhin, B., Van Der Wijst, K.I., Winter, G., Witting, M., Birt, A., Ha, M., Romero, J., Kim, J., Haites, E.F.,
 326 Jung, Y., Stavins, R., Birt, A., Ha, M., Orendain, D.J.A., Ignon, L., Park, S., Park, Y., Reisinger, A., Cammaramo, D.,
 327 Fischlin, A., Fuglestvedt, J.S., Hansen, G., Ludden, C., Masson-Delmotte, V., Matthews, J.R., Mintenbeck, K., Pirani, A.,
 328 Poloczanska, E., Leprince-Ringuet, N., Péan, C., 2023. IPCC, 2023: Climate Change 2023: Synthesis Report. Contribution
 329 of Working Groups I, II and III to the Sixth Assessment Report of the Intergovernmental Panel on Climate Change [Core
 330 Writing Team, H. Lee and J. Romero (eds.)]. IPCC, Geneva, Switzerland. Technical Report. Intergovernmental Panel on
 331 Climate Change (IPCC). URL: <https://www.ipcc.ch/report/ar6/syr/>.
 332 Crausbay, S.D., Ramirez, A.R., Carter, S.L., Cross, M.S., Hall, K.R., Bathke, D.J., Betancourt, J.L., Colt, S., Cravens, A.E.,
 333 Dalton, M.S., Dunham, J.B., Hay, L.E., Hayes, M.J., McEvoy, J., McNutt, C.A., Moritz, M.A., Nislow, K.H., Raheem, N.,
 334 Sanford, T., 2017. Defining Ecological Drought for the Twenty-First Century. *Bulletin of the American Meteorological Society*
 335 98, 2543–2550. URL: <https://journals.ametsoc.org/view/journals/bams/98/12/bams-d-16-0292.1.xml>, doi:[10.1175/BAMS-D-16-0292.1](https://doi.org/10.1175/BAMS-D-16-0292.1). publisher: American Meteorological Society.
 336 Cui, A., Li, J., Zhou, Q., Zhu, R., Liu, H., Wu, G., Li, Q., 2021. Use of a multiscalar GRACE-based standardized terrestrial
 337 water storage index for assessing global hydrological droughts. *Journal of Hydrology* 603, 126871. URL: <https://linkinghub.elsevier.com/retrieve/pii/S0022169421009215>, doi:[10.1016/j.jhydrol.2021.126871](https://doi.org/10.1016/j.jhydrol.2021.126871).
 338 Didan, K., 2015. MOD13Q1 MODIS/Terra Vegetation Indices 16-Day L3 Global 250m SIN Grid V006. Technical Report.
 339 NASA EOSDIS Land Processes DAAC. doi:<http://dx.doi.org/10.5067/MODIS/MOD13Q1.006>.
 340 Fernández, F.J., Vásquez-Lavín, F., Ponce, R.D., Garreaud, R., Hernández, F., Link, O., Zambrano, F., Hanemann, M., 2023.
 341 The economics impacts of long-run droughts: Challenges, gaps, and way forward. *Journal of Environmental Management*
 342 344, 118726. URL: <https://linkinghub.elsevier.com/retrieve/pii/S0301479723015141>, doi:[10.1016/j.jenvman.2023.118726](https://doi.org/10.1016/j.jenvman.2023.118726).
 343 Friedl, M., Sulla-Menashe, D., 2019. MCD12Q1 MODIS/Terra+Aqua Land Cover Type Yearly L3 Global 500m SIN Grid V006
 344 [Data set]. NASA EOSDIS Land Processes DAAC. doi:<http://dx.doi.org/10.5067/MODIS/MCD12Q1.006>.
 345 Fuentes, I., Fuster, R., Avilés, D., Vervoort, W., 2021. Water scarcity in central Chile: the effect of climate and land cover
 346 changes on hydrologic resources. *Hydrological Sciences Journal* 66, 1028–1044. URL: <https://www.tandfonline.com/doi/full/10.1080/02626667.2021.1903475>, doi:[10.1080/02626667.2021.1903475](https://doi.org/10.1080/02626667.2021.1903475).
 347 Garreaud, R., Alvarez-Garreton, C., Barichivich, J., Boisier, J.P., Christie, D., Galleguillos, M., LeQuenne, C., McPhee, J.,
 348 Zambrano-Bigiarini, M., 2017. The 2010–2015 mega drought in Central Chile: Impacts on regional hydroclimate and
 349 vegetation. *Hydrology and Earth System Sciences Discussions* 2017, 1–37. URL: <http://www.hydrol-earth-syst-sci-discuss.net/hess-2017-191/>, doi:[10.5194/hess-2017-191](https://doi.org/10.5194/hess-2017-191).
 350 Garreaud, R.D., 2009. The Andes climate and weather. *Advances in Geosciences* 22, 3–11. URL: <https://adgeo.copernicus.org/articles/22/3/2009/>, doi:[10.5194/adgeo-22-3-2009](https://doi.org/10.5194/adgeo-22-3-2009).
 351 Garreaud, R.D., Boisier, J.P., Rondanelli, R., Montecinos, A., Sepúlveda, H.H., Veloso-Aguila, D., 2020. The Central Chile
 352 Mega Drought (2010–2018): A climate dynamics perspective. *International Journal of Climatology* 40, 421–439. URL:
 353 <https://rmets.onlinelibrary.wiley.com/doi/10.1002/joc.6219>, doi:[10.1002/joc.6219](https://doi.org/10.1002/joc.6219).
 354 Grekousis, G., Mountrakis, G., Kavouras, M., 2015. An overview of 21 global and 43 regional land-cover mapping products.
 355 International Journal of Remote Sensing 36, 5309–5335. URL: <https://www.tandfonline.com/doi/full/10.1080/01431161.2015.1093195>, doi:[10.1080/01431161.2015.1093195](https://doi.org/10.1080/01431161.2015.1093195).
 356 Hao, Z., AghaKouchak, A., 2013. Multivariate Standardized Drought Index: A parametric multi-index model. *Advances in Water
 357 Resources* 57, 12–18. URL: <https://linkinghub.elsevier.com/retrieve/pii/S0309170813000493>, doi:[10.1016/j.advwatres.2013.03.009](https://doi.org/10.1016/j.advwatres.2013.03.009).
 358 Hargreaves, G.H., 1994. Defining and Using Reference Evapotranspiration. *Journal of Irrigation and Drainage Engineering* 120,
 359 1132–1139. URL: [https://ascelibrary.org/doi/10.1061/\(ASCE\)0733-9437\(1994\)120:6\(1132\)](https://ascelibrary.org/doi/10.1061/(ASCE)0733-9437(1994)120:6(1132)), doi:[10.1061/\(ASCE\)0733-9437\(1994\)120:6\(1132\)](https://doi.org/10.1061/(ASCE)0733-9437(1994)120:6(1132)).
 360 Hijmans, R.J., 2023. terra: Spatial Data Analysis. URL: <https://CRAN.R-project.org/package=terra>.
 361 Ho, T.K., 1995. Random decision forests, in: Proceedings of 3rd international conference on document analysis and recognition,
 362 IEEE. pp. 278–282.
 363 Hobbins, M.T., Wood, A., McEvoy, D.J., Huntington, J.L., Morton, C., Anderson, M., Hain, C., 2016. The Evaporative Demand
 364 Drought Index. Part I: Linking Drought Evolution to Variations in Evaporative Demand. *Journal of Hydrometeorology* 17,
 365 1745–1761. URL: <http://journals.ametsoc.org/doi/10.1175/JHM-D-15-0121.1>, doi:[10.1175/JHM-D-15-0121.1](https://doi.org/10.1175/JHM-D-15-0121.1).
 366 Hoerl, A.E., Kennard, R.W., 1970. Ridge Regression: Biased Estimation for Nonorthogonal Problems. *Technometrics* 12, 55–67.

- 375 URL: <http://www.tandfonline.com/doi/abs/10.1080/00401706.1970.10488634>, doi:[10.1080/00401706.1970.10488634](https://doi.org/10.1080/00401706.1970.10488634).
- 376 Hufkens, K., Stauffer, R., Campitelli, E., 2019. The ecwmfr package: an interface to ECMWF API endpoints. URL: <https://bluegreen-labs.github.io/ecmwfr/>.
- 377 IPCC, 2013. Climate Change 2013: The Physical Science Basis. Contribution of Working Group I to the Fifth Assessment Report of the Intergovernmental Panel on Climate Change. Cambridge University Press, Cambridge, UK; New York, USA.
- 378 URL: www.climatechange2013.org, doi:[10.1017/CBO9781107415324](https://doi.org/10.1017/CBO9781107415324).
- 379 Kendall, M., 1975. Rank correlation methods (4th ed. 2d impression). Griffin.
- 380 Kogan, F.N., 1995. Application of vegetation index and brightness temperature for drought detection. Advances in Space Research 15, 91–100. doi:[10.1016/0273-1177\(95\)00079-T](https://doi.org/10.1016/0273-1177(95)00079-T).
- 381 Luo, L., Apps, D., Arcand, S., Xu, H., Pan, M., Hoerling, M., 2017. Contribution of temperature and precipitation anomalies to the California drought during 2012–2015. Geophysical Research Letters 44, 3184–3192. URL: <https://agupubs.onlinelibrary.wiley.com/doi/10.1002/2016GL072027>, doi:[10.1002/2016GL072027](https://doi.org/10.1002/2016GL072027).
- 382 Ma, S., Wu, Q., Wang, J., Zhang, S., 2017. Temporal Evolution of Regional Drought Detected from GRACE TWSA and CCI SM in Yunnan Province, China. Remote Sensing 2017, Vol. 9, Page 1124 9, 1124. URL: <https://www.mdpi.com/2072-4292/9/11/1124>, doi:[10.3390/RS9111124](https://doi.org/10.3390/RS9111124). publisher: Multidisciplinary Digital Publishing Institute.
- 383 McEvoy, D.J., Huntington, J.L., Hobbins, M.T., Wood, A., Morton, C., Anderson, M., Hain, C., 2016. The Evaporative Demand Drought Index. Part II: CONUS-Wide Assessment against Common Drought Indicators. Journal of Hydrometeorology 17, 1763–1779. URL: <http://journals.ametsoc.org/doi/10.1175/JHM-D-15-0122.1>, doi:[10.1175/JHM-D-15-0122.1](https://doi.org/10.1175/JHM-D-15-0122.1).
- 384 McKee, T.B., Doesken, N.J., Kleist, J., 1993. The relationship of drought frequency and duration to time scales. In: Proceedings of the Ninth Conference on Applied Climatology. American Meteorological Society , 179–184.
- 385 Meroni, M., Rembold, F., Fasbender, D., Vrieling, A., 2017. Evaluation of the Standardized Precipitation Index as an early predictor of seasonal vegetation production anomalies in the Sahel. Remote Sensing Letters 8, 301–310. URL: <https://www.tandfonline.com/doi/full/10.1080/2150704X.2016.1264020>, doi:[10.1080/2150704X.2016.1264020](https://doi.org/10.1080/2150704X.2016.1264020).
- 386 Miranda, A., Lara, A., Altamirano, A., Di Bella, C., González, M.E., Julio Camarero, J., 2020. Forest browning trends in response to drought in a highly threatened mediterranean landscape of South America. Ecological Indicators 115, 106401. URL: <https://linkinghub.elsevier.com/retrieve/pii/S1470160X20303381>, doi:[10.1016/j.ecolind.2020.106401](https://doi.org/10.1016/j.ecolind.2020.106401).
- 387 Miranda, A., Syphard, A.D., Berdugo, M., Carrasco, J., Gómez-González, S., Ovalle, J.F., Delpiano, C.A., Vargas, S., Squeo, F.A., Miranda, M.D., Dobbs, C., Mentler, R., Lara, A., Garreaud, R., 2023. Widespread synchronous decline of Mediterranean-type forest driven by accelerated aridity. Nature Plants 9, 1810–1817. URL: <https://www.nature.com/articles/s41477-023-01541-7>, doi:[10.1038/s41477-023-01541-7](https://doi.org/10.1038/s41477-023-01541-7).
- 388 Muñoz-Sabater, J., Dutra, E., Agustí-Panareda, A., Albergel, C., Arduini, G., Balsamo, G., Boussetta, S., Choulga, M., Harrigan, S., Hersbach, H., Martens, B., Miralles, D.G., Piles, M., Rodríguez-Fernández, N.J., Zsoter, E., Buontempo, C., Thépaut, J.N., 2021. ERA5-Land: a state-of-the-art global reanalysis dataset for land applications. Earth System Science Data 13, 4349–4383. URL: <https://essd.copernicus.org/articles/13/4349/2021/>, doi:[10.5194/essd-13-4349-2021](https://doi.org/10.5194/essd-13-4349-2021).
- 389 Narasimhan, B., Srinivasan, R., 2005. Development and evaluation of Soil Moisture Deficit Index (SMDI) and Evapotranspiration Deficit Index (ETDI) for agricultural drought monitoring. Agricultural and Forest Meteorology 133, 69–88. URL: <https://linkinghub.elsevier.com/retrieve/pii/S0168192305001565>, doi:[10.1016/j.agrformet.2005.07.012](https://doi.org/10.1016/j.agrformet.2005.07.012).
- 390 Nouri, M., 2023. Drought Assessment Using Gridded Data Sources in Data-Poor Areas with Different Aridity Conditions. Water Resources Management 37, 4327–4343. URL: <https://link.springer.com/10.1007/s11269-023-03555-4>, doi:[10.1007/s11269-023-03555-4](https://doi.org/10.1007/s11269-023-03555-4).
- 391 Paruelo, J.M., Texeira, M., Staiano, L., Mastrángelo, M., Amdan, L., Gallego, F., 2016. An integrative index of Ecosystem Services provision based on remotely sensed data. Ecological Indicators 71, 145–154. URL: <https://www.sciencedirect.com/science/article/pii/S1470160X16303843>, doi:[10.1016/j.ecolind.2016.06.054](https://doi.org/10.1016/j.ecolind.2016.06.054). publisher: Elsevier.
- 392 Pebesma, E., 2018. Simple Features for R: Standardized Support for Spatial Vector Data. The R Journal 10, 439–446. URL: <https://doi.org/10.32614/RJ-2018-009>, doi:[10.32614/RJ-2018-009](https://doi.org/10.32614/RJ-2018-009).
- 393 Pebesma, E., Bivand, R., 2023. Spatial Data Science: With applications in R. Chapman and Hall/CRC, London. URL: <https://r-spatial.org/book/>.
- 394 R Core Team, 2023. R: A Language and Environment for Statistical Computing. R Foundation for Statistical Computing, Vienna, Austria. URL: <https://www.R-project.org/>.
- 395 Schucknecht, A., Meroni, M., Kayitakire, F., Boureima, A., Schucknecht, A., Meroni, M., Kayitakire, F., Boureima, A., 2017. Phenology-Based Biomass Estimation to Support Rangeland Management in Semi-Arid Environments. Remote Sensing 9, 463. URL: <https://www.mdpi.com/2072-4292/9/5/463>, doi:[10.3390/rs9050463](https://doi.org/10.3390/rs9050463). publisher: Multidisciplinary Digital Publishing Institute.
- 396 Sen, P.K., 1968. Estimates of the Regression Coefficient Based on Kendall's Tau. Journal of the American Statistical Association 63, 1379–1389. URL: <http://www.tandfonline.com/doi/abs/10.1080/01621459.1968.10480934>, doi:[10.1080/01621459.1968.10480934](https://doi.org/10.1080/01621459.1968.10480934).
- 397 Seneviratne, S and Zhang, X.a.A.M.a.B.W.a.D.C.a.L.A.a.G.S.a.I.I.a.K.J.a.L.S.a.O.F.a.P.I.a.S.M.a.V.S.S.a.W.M.a.Z..M.D.B.a.V.a.O., 2021. Weather and Climate Extreme Events in a Changing Climate. Cambridge University Press. In Press. Publication Title: Climate Change 2021: The Physical Science Basis. Contribution of Working Group I to the Sixth Assessment Report of the Intergovernmental Panel on Climate Change.
- 398 Slette, I.J., Post, A.K., Awad, M., Even, T., Punzalan, A., Williams, S., Smith, M.D., Knapp, A.K., 2019. How ecologists define drought, and why we should do better. Global Change Biology 25, 3193–3200. URL: <https://onlinelibrary.wiley.com/doi/10.1111/gcb.14747>, doi:[10.1111/gcb.14747](https://doi.org/10.1111/gcb.14747).
- 399 Souza, A.G.S.S., Ribeiro Neto, A., Souza, L.L.D., 2021. Soil moisture-based index for agricultural drought assessment: SMADI application in Pernambuco State-Brazil. Remote Sensing of Environment 252, 112124. URL: <https://linkinghub.elsevier.com>.

- 440 com/retrieve/pii/S0034425720304971, doi:10.1016/j.rse.2020.112124.
- 441 Tibshirani, R., Bien, J., Friedman, J., Hastie, T., Simon, N., Taylor, J., Tibshirani, R.J., 2010. Strong rules for discarding
442 predictors in lasso-type problems. URL: <http://arxiv.org/abs/1011.2234>.
- 443 Tran, H.T., Campbell, J.B., Wynne, R.H., Shao, Y., Phan, S.V., 2019. Drought and Human Impacts on Land Use and Land
444 Cover Change in a Vietnamese Coastal Area. *Remote Sensing* 2019, Vol. 11, Page 333 11, 333. URL: <https://www.mdpi.com/2072-4292/11/3/333/htm>, doi:10.3390/RS11030333. publisher: Multidisciplinary Digital Publishing Institute.
- 445 Urrutia-Jalabert, R., González, M.E., González-Reyes, , Lara, A., Garreaud, R., 2018. Climate variability and forest fires in
446 central and south-central Chile. *Ecosphere* 9, e02171. URL: <https://esajournals.onlinelibrary.wiley.com/doi/10.1002/ecs2.2171>, doi:10.1002/ecs2.2171.
- 447 Van Loon, A.F., Gleeson, T., Clark, J., Van Dijk, A.I., Stahl, K., Hannaford, J., Di Baldassarre, G., Teuling, A.J., Tallaksen,
448 L.M., Uijlenhoet, R., Hannah, D.M., Sheffield, J., Svoboda, M., Verbeiren, B., Wagener, T., Rangecroft, S., Wanders, N.,
449 Van Lanen, H.A., 2016. Drought in the Anthropocene. *Nature Geoscience* 9, 89–91. doi:10.1038/ngeo2646.
- 450 Venegas-González, A., Juñent, F.R., Gutiérrez, A.G., Filho, M.T., 2018. Recent radial growth decline in response to increased
451 drought conditions in the northernmost Nothofagus populations from South America. *Forest Ecology and Management* 409,
452 94–104. URL: <https://linkinghub.elsevier.com/retrieve/pii/S0378112717313993>, doi:10.1016/j.foreco.2017.11.006.
- 453 Vicente-Serrano, S.M., Beguería, S., López-Moreno, J.I., 2010. A multiscalar drought index sensitive to global warming: The
454 standardized precipitation evapotranspiration index. *Journal of Climate* 23, 1696–1718. URL: <http://dx.doi.org/10.1175/2009JCLI2909.1>, doi:10.1175/2009JCLI2909.1.
- 455 Vicente-Serrano, S.M., Miralles, D.G., Domínguez-Castro, F., Azorin-Molina, C., El Kenawy, A., McVicar, T.R., Tomás-
456 Burguera, M., Beguería, S., Maneta, M., Peña-Gallardo, M., 2018. Global Assessment of the Standardized Evapotranspiration
457 Deficit Index (SEDI) for Drought Analysis and Monitoring. *Journal of Climate* 31, 5371–5393. URL: <https://journals.ametsoc.org/doi/10.1175/JCLI-D-17-0775.1>, doi:10.1175/JCLI-D-17-0775.1.
- 458 Vicente-Serrano, S.M., Peña-Angulo, D., Beguería, S., Domínguez-Castro, F., Tomás-Burguera, M., Noguera, I., Gimeno-Sotelo,
459 L., El Kenawy, A., 2022. Global drought trends and future projections. *Philosophical Transactions of the Royal Society A:
460 Mathematical, Physical and Engineering Sciences* 380, 20210285. URL: <https://royalsocietypublishing.org/doi/10.1098/rsta.2021.0285>, doi:10.1098/rsta.2021.0285.
- 461 Wang, M., Menzel, L., Jiang, S., Ren, L., Xu, C.Y., Cui, H., 2023. Evaluation of flash drought under the impact of heat wave
462 events in southwestern Germany. *Science of The Total Environment* 904, 166815. URL: <https://linkinghub.elsevier.com/retrieve/pii/S0048969723054402>, doi:10.1016/j.scitotenv.2023.166815.
- 463 West, H., Quinn, N., Horswell, M., 2019. Remote sensing for drought monitoring \& impact assessment: Progress, past
464 challenges and future opportunities. *Remote Sensing of Environment* 232. doi:10.1016/j.rse.2019.111291. publisher:
465 Elsevier Inc.
- 466 Wilhite, D.A., Glantz, M.H., 1985. Understanding: The drought phenomenon: The role of definitions. *Water International* 10,
467 111–120. URL: <http://dx.doi.org/10.1080/02508068508686328>, doi:10.1080/02508068508686328.
- 468 Wilks, D.S., 2011. Empirical distributions and exploratory data analysis. *Statistical Methods in the Atmospheric Sciences* 100.
- 469 WMO, Svoboda, M., Hayes, M., Wood, D.A., 2012. Standardized Precipitation Index User Guide. WMO, Geneva. URL:
470 http://library.wmo.int/opac/index.php?lvl=notice_display&id=13682. series Title: WMO Publication Title: WMO-No.
471 1090 © Issue: 1090.
- 472 Zambrano, F., 2023. Four decades of satellite data for agricultural drought monitoring throughout the growing season in Central
473 Chile, in: Vijay P. Singh Deepak Jhajharia, R.M., Kumar, R. (Eds.), *Integrated Drought Management*, Two Volume Set.
474 CRC Press, p. 28.
- 475 Zambrano, F., Lillo-Saavedra, M., Verbist, K., Lagos, O., 2016. Sixteen years of agricultural drought assessment of the
476 biobío region in chile using a 250 m resolution vegetation condition index (VCI). *Remote Sensing* 8, 1–20. URL: <http://www.mdpi.com/2072-4292/8/6/530>, doi:10.3390/rs8060530. publisher: Multidisciplinary Digital Publishing Institute.
- 477 Zambrano, F., Vrieling, A., Nelson, A., Meroni, M., Tadesse, T., 2018. Prediction of drought-induced reduction of agricultural
478 productivity in Chile from MODIS, rainfall estimates, and climate oscillation indices. *Remote Sensing of Environment*
479 219, 15–30. URL: <https://www.sciencedirect.com/science/article/pii/S0034425718304541>, doi:10.1016/j.rse.2018.10.006.
480 publisher: Elsevier.
- 481 Zhao, Y., Feng, D., Yu, L., Wang, X., Chen, Y., Bai, Y., Hernández, H.J., Galleguillos, M., Estades, C., Biging, G.S., Radke,
482 J.D., Gong, P., 2016. Detailed dynamic land cover mapping of Chile: Accuracy improvement by integrating multi-temporal
483 data. *Remote Sensing of Environment* 183, 170–185. URL: <https://linkinghub.elsevier.com/retrieve/pii/S0034425716302188>,
484 doi:10.1016/j.rse.2016.05.016.